

## MAGNETAR CENTRAL ENGINE AND POSSIBLE GRAVITATIONAL WAVE EMISSION OF NEARBY SHORT GRB 160821B

HOU-JUN LÜ<sup>1,2</sup>, HAI-MING ZHANG<sup>1,2</sup>, SHU-QING ZHONG<sup>1,2</sup>, SHU-JIN HOU<sup>3</sup>, HUI SUN<sup>4</sup>, JARED RICE<sup>5</sup>, AND EN-WEI LIANG<sup>1,2</sup>

## ABSTRACT

GRB 160821B is a short gamma-ray burst (GRB) at redshift  $z = 0.16$ , with a duration less than 1 second and without detection of any “extended emission” up to more than 100 seconds in both *Swift*/BAT and *Fermi*/GBM bands. An X-ray plateau with a sharp drop 180 seconds after the BAT trigger was observed with *Swift*/XRT. No supernova or kilo-nova signature was detected. Assuming the central engine of this SGRB is a recently born supra-massive magnetar, we can explain the SGRB as jet radiation and its X-ray plateau as the internal energy dissipation of the pulsar wind as it spins down. We constrain its surface magnetic field as  $B_p < 3.12 \times 10^{16}$  G and initial spin period as  $P_0 < 8.5 \times 10^{-3}$  seconds. Its equation of state is consistent with the GM1 model with  $M_{\text{TOV}} \sim 2.37M_\odot$  and ellipticity  $\epsilon < 0.07$ . Its gravitational wave (GW) radiation may be detectable with the future Einstein Telescope, but is much weaker than the current detectability limit of advanced-LIGO. The GW radiation of such an event would be detectable by advanced-LIGO if it occurred at a distance of 100 Mpc ( $z = 0.023$ ).

*Subject headings:* gamma rays burst: individual (160821B)

## 1. INTRODUCTION

The progenitors of short gamma-ray bursts (SGRBs), which have a hard spectrum and short duration (Kouveliotou et al. 1993), remain elusive (Zhang 2011). Several lines of observational evidence, e.g. low level of star formation (Barthelmy et al. 2005; Berger et al. 2005; Gehrels et al. 2005), a large offset from the center of the host galaxy (e.g. Fox et al. 2005; Fong et al. 2010), as well as the non-association of bright supernovae (SNe) with short GRBs (Berger 2014 and references therein), suggest that SGRBs may form in compact star mergers, such as neutron star–neutron star mergers (NS–NS, Paczyński 1986; Eichler et al. 1989), neutron star–black hole mergers (NS–BH, Paczyński 1991), or black hole–black hole mergers (BH–BH; Zhang 2016). The coalescence of two compact stars is also expected to be a strong source of gravitational wave (GW) radiation, and such systems are the main targets of the advanced Laser Interferometer Gravitational-wave Observatory (LIGO)/Virgo detectors. Two GW events (GW 150914 and GW 151226) and one GW candidate (LVT 151012) were detected with LIGO and are proposed black hole binary mergers (Abbott et al. 2016a,b). Electromagnetic (EM) transients associated with gravitational wave bursts (GWBs) have not been confidently detected, although associations of weak EM counterparts with these GW events were claimed (Connaughton et al. 2016). Since the two GW events are believed to be from

BH–BH systems, it is still highly debated whether or not the merger of a BH–BH system can be accompanied by an EM counterpart (Zhang 2016; Zhang et al. 2016; Connaughton et al. 2016; Xiong 2016). Further observations are required to confirm the existence of BH–BH EM counterparts.

NS–NS mergers as the progenitors of SGRBs have been extensively studied. Depending on the nascent NS mass ( $M_p$ ), two possible outcomes of the merger are expected. One possibility is a black hole, which forms when  $M_p$  is much greater than the maximum non-rotating mass ( $M_{\text{TOV}}$ , Rosswog et al. 2003; Rezzolla et al. 2011; Ravi & Lasky 2014). Another possibility is a rapidly spinning, strongly magnetized neutron star (“millisecond magnetar”), in the case where  $M_p$  is less than  $M_{\text{TOV}}$  but greater than  $M_{\text{max}}$  (the maximum gravitational mass) (Usov 1992; Thompson 1994; Dai & Lu 1998a,b; Zhang & Mészáros 2001; Metzger et al. 2008, 2011; Bucciantini et al. 2012). The post-merger evolution of magnetars also depends on the mass lying between  $M_p$  and  $M_{\text{TOV}}$ . One possible channel is a magnetar in an equilibrium state which injects energy from the magnetar wind via loss of rotation energy for  $M_p \leq M_{\text{TOV}}$  (Giacomazzo & Perna 2013). This well explains the long lasting energy injection phase observed with the Swift X-Ray Telescope (XRT; Burrows et al. 2004). Another evolving channel is that of a supra-massive NS, which may survive if  $M_{\text{TOV}} < M_p < M_{\text{max}}$ , when magnetic braking and viscosity compel the star into uniform rotation. As the period of the magnetar decreases via rotational energy loss, the maximum gravitational mass decreases. The magnetar collapses into a black hole when its centrifugal force cannot balance the gravitational force (Duez et al. 2006; Ravi & Lasky 2014). Theoretically, it is expected that a Poynting-flux dominated outflow is driven by the injected wind as the magnetar spins down (e.g. Dai & Lu 1998a; Zhang & Mészáros 2001). The observed X-ray “internal plateau” (the rapid flux drop off at the end of

<sup>1</sup> GXU-NAOC Center for Astrophysics and Space Sciences, Department of Physics, Guangxi University, Nanning 530004, China; lhj@gxu.edu.edu

<sup>2</sup> Guangxi Key Laboratory for Relativistic Astrophysics, Nanning, Guangxi 530004, China

<sup>3</sup> College of Physics and Electronic Engineering, Nanyang Normal University, Nanyang, Henan 473061, China

<sup>4</sup> Department of Astronomy, School of Physics, Peking University, Beijing 100871, China

<sup>5</sup> Department of Physics and Astronomy, University of Nevada Las Vegas, NV 89154, USA

the plateau emission with a decay slope  $\alpha > 3$ )<sup>6</sup> with XRT in a few long and short GRBs (Troja et al. 2007; Lyons et al. 2010; Rowlinson et al. 2010, 2013; Lü et al. 2015; Du et al. 2016) may be evidence for this evolution channel. The rapid decay following the plateau cannot be accommodated in any external shock model and can be attributed to internal dissipation of a central engine wind, which is likely a signature of the collapse of a supra-massive magnetar central engine into a black hole (Troja et al. 2007; Liang et al. 2007; Lyons et al. 2010; Lü & Zhang 2014; Lü et al. 2015). It has also been proposed that this phenomenon may be accompanied by a fast radio transient, i.e., fast radio burst (FRB, Lorimer et al. 2007; Zhang 2014).

In NS-NS merger models, it is predicted that EM signals can not be avoided after the merger due to the high magnetic field strength at the NS surface (Metzger & Berger 2012). In addition, a NS-NS merger would also lose energy via gravitational wave quadrupole emission (Fan et al. 2013; Lasky et al. 2014; Lasky & Glampedakis 2016). Therefore, hunting for possible associations of SGRBs with GW events is interesting. The LIGO team has searched for such associations for many years, but no events have been reported. Comparing the BH-BH mergers with the associated GWBs detected with the advanced-LIGO, the energy lost via GWB in these systems would be much larger than that expected in NS-NS merger systems (Corsi & Mészáros 2009; Hild et al. 2011; Fan et al. 2013). Therefore, the advanced-LIGO detection rate for NS-NS mergers should be much lower than that of BH-BH merger systems.

GRB 160821B is a nearby bright SGRB with a redshift of  $z = 0.16$ . This paper dedicates analysis of its multi-wavelength data and constrains the properties of its central engine as well as its possible GW radiation. We present our data reduction from *Swift* and *Fermi* observations in §2. In §3, we compare the properties of GRB 160821B with other SGRBs. The derived parameters for a magnetar central engine and the equation of state of newly-born NSs are presented in §4. In §5, we present a constraint on the ellipticity of the NS-NS system and the probability of detectable gravitational wave radiation. Conclusions are drawn in §6 with some additional discussion. Throughout the paper, a concordance cosmology with parameters  $H_0 = 71 \text{ km s}^{-1} \text{ Mpc}^{-1}$ ,  $\Omega_M = 0.30$ , and  $\Omega_\Lambda = 0.70$  is adopted.

## 2. DATA REDUCTION AND ANALYSIS

### 2.1. Swift data reduction

GRB 160821B triggered the Burst Alert Telescope (BAT) at 22:29:13 UT on 2016 August 21 (Siegel et al. 2016). We developed an IDL script to automatically download the *Swift* BAT data. We use the standard HEASOFT tools (version 6.12) to process the data. We run *bateconvert* from the HEASOFT software release to obtain the energy scale for the BAT events. The light curves and spectra are extracted by running *batbinevt* (Sakamoto et al. 2007). Then, we calculate the cumulative distribution of the source counts using the arrival time of a fraction between 5 and 95 per cent of the total counts to define  $T_{90}$ . The time bin size is fixed to

64 ms in this case due to the short duration. The background is extracted using two time intervals, one before and one after the burst. We model the background as Poisson noise, which is the standard background model for prompt emission. We invoked Xspec to fit the spectra. For technical details please refer to Sakamoto et al. (2007). XRT began observing the field 57 seconds after the BAT trigger (Siegel et al. 2016). We made use of the public data from the *Swift* archive<sup>7</sup>. The Ultra-Violet Optical Telescope (UVOT; Roming et al. 2005) observed the field at  $T_0 + 76 \text{ s}$ , but no optical afterglow was consistent with the XRT position (Evans et al. 2016). There was also no detection in the initial UVOT exposures (Xu et al. 2016). Preliminary,  $3\sigma$  upper limits data are obtained by using the UVOT photometric system for the first finding chart (FC) exposure (Breeveld et al. 2016). On the other hand,  $r$ - and  $z$ -band afterglow images were obtained by using William Herschel Telescope on La Palma (Levan et al. 2016). In the spectrum of the candidate host galaxy several prominent emission lines were found ( $H\beta$ ,  $[OIII]$  and  $H\alpha$ ), at a redshift of  $z = 0.16$ . The physical offset of the afterglow from the candidate host galaxy is approximately 15 kpc (Levan et al. 2016).

### 2.2. Fermi data reduction

*Fermi* Gamma-ray Burst Monitor (GBM) triggered and located GRB 160821B at 22:29:13.33 UT on 21 August 2016 (Stanbro et al. 2016). GBM has 12 sodium iodide (NaI) and two bismuth germanate (BGO) scintillation detectors, covering the energy range 8 keV to 40 MeV (Meegan et al. 2009). We downloaded GBM data of this GRB from the public science support center at the official Fermi web site<sup>8</sup>. Each of the GBM detectors collected the data with three different types: CTIME, CSPEC, and TTE. Then, we extracted the light curves and performed spectral analysis based on the package *gtBurst*. By invoking the *heasoft* command *fselect* and the *ScienceTools* command *gtbin*, we extracted light curves with a time-bin of 64 ms in a user-specified energy band from the GBM. We clicked “Tasks → Make spectra for XSPEC” in *gtBurst* to extract the source spectrum of the GBM data. The background spectra are extracted from the time intervals before and after the prompt emission phase, modeled with a polynomial function, and the source spectrum is extracted by applying the background model to the prompt emission phase. This GRB occurred right at the edge of the Large Area Telescope (LAT) field-of-view (Atwood et al. 2009), about 61 degrees from boresight. So we do not expect to detect the high-energy signal if it exists.

### 2.3. Swift and Fermi data analysis

As shown in Fig.1, the BAT light curve shows a single short peak with duration  $T_{90} = 0.48 \pm 0.07 \text{ s}$ , and there is no evidence of extended emission detected in the BAT energy range up to 100 s after the BAT trigger ( $T_0$ ). The time-integrated BAT spectrum can be fit by a single power law with photon index  $\Gamma_\gamma = 1.98 \pm 0.11$ . The BAT band (15–150 keV)

<sup>6</sup> Throughout the paper we adopt the convention  $F_\nu \propto t^{-\alpha} \nu^{-\beta}$ .

<sup>7</sup> <http://www.swift.ac.uk/xrtcurves/00709357>

<sup>8</sup> <http://fermi.gsfc.nasa.gov/ssc/data/>

peak flux is  $(1.7 \pm 0.2)$  photons  $\text{cm}^{-2} \text{s}^{-1}$ , and the total fluence is  $(1.1 \pm 0.1) \times 10^{-7}$  erg  $\text{cm}^{-2}$  (Palmer et al. 2016). The GBM light curve of GRB 160821B is also shown in Figure 1 with a 64 ms time-bin. The profile of light curve is similar with BAT data, has a bright peak with duration  $T_{90} \sim 1.2$  s in 8–1000 keV range. The GBM spectra can be fit by a power law function due to lack high energy photons<sup>9</sup>. Here, we joint fit the time-averaged spectra of *Fermi*/GBM+*Swift*/BAT with a power-law model, and found  $\Gamma_{\text{BAT+GBM}} = 1.88 \pm 0.12$  with  $\chi^2 = 0.84$  (Fig. 2). The total fluence in 8–10000 keV is  $(2.52 \pm 0.19) \times 10^{-6}$  erg  $\text{cm}^{-2}$ . The isotropic energy  $E_{\gamma, \text{iso}} = (2.1 \pm 0.2) \times 10^{50}$  erg.

Norris et al (2000) discovered an anti-correlation between GRB peak luminosity and the delay time ( $t_{\text{lag}}$ ) in different energy bands, meaning softer photons usually arrive later than hard photons. This spectral lag is always significant in long-duration GRBs (Norris et al. 2000; Gehrels et al. 2006; Liang et al. 2006), but is typically negligible in short-duration GRBs (Norris & Bonnell 2006; Zhang et al. 2009). We extracted 4 ms binned light curves in the following three BAT energy bands: 15–25 keV, 25–50 keV, 50–100 keV<sup>10</sup>. Then, we used the cross-correlation function method (CCF; Norris et al. 2000; Ukwatta et al. 2010) to calculate the lags between 25–50 keV and 50–100 keV light curves. In order to address the questions of whether the short GRB 160821B is consistent with typical Type I and other short-hard GRBs with in the spectral lag distribution. Figure 4 shown the peak luminosity as function of spectral lag for typical Type II, Type I, other short-hard, and GRB 160821B. Here, Type II GRBs are corresponding to confirmed supernova (SN) association, or have a high specific star formation rate (SSFR) and do not have a large offset from the galaxy center. On the contrary, Type I GRBs are occurred in elliptical or early type host galaxy without SN signature, or has a relatively low local SSFR and large offset from the host galaxy center. For the other short-hard GRBs, do not satisfy neither of the two criteria of the Type I sample, and do not have their host galaxy identified, but with a short duration, hard spectral (Zhang et al. 2009). Type II GRBs sample are from Norris & Bonnell (2006), and give the best power-law model fitting with  $2\sigma$  region of the fitting. Type I and other short-hard GRBs are collected from Zhang et al (2009). For GRB 160821B, we found  $t_{\text{lag}} = (10 \pm 6)$  ms, which is consistent with result of Palmer et al (2016). It is deviated from  $2\sigma$  region of the Type II GRBs fitting, but both peak luminosity and lag value of this case is comparable with Type I GRBs.

The initial X-ray light curve is best fit by a broken power law, which reads

$$F = F_0 \left[ \left( \frac{t}{t_b} \right)^{\omega\alpha_1} + \left( \frac{t}{t_b} \right)^{\omega\alpha_2} \right]^{-1/\omega}, \quad (1)$$

where  $\omega$  describes the sharpness of the break and is taken to be 3 in this analysis (Liang et al. 2007). There is an

<sup>9</sup> Stanbro et al. (2016) find that the spectrum can be fit by a power law function with an exponential high-energy cutoff. The power law index is  $\Gamma_{\text{GBM}} = -1.31 \pm 0.6$ , and the cutoff energy  $E_p = 84 \pm 19$  keV.

<sup>10</sup> The signal in 100–150 keV is too weak to be extracted, so we do not consider the emission in this energy band.

initial decay slope  $\alpha_1 = 0.21 \pm 0.14$ , followed by a steeper decay of  $\alpha_2 = 4.52 \pm 0.45$  with a break time  $t_b = 180 \pm 46$  seconds after the BAT trigger. No significant X-ray flare was detected during the observational time. The X-ray spectrum in the 0.3–10 keV energy band is best fit by an absorbed power law with  $\Gamma_X = 1.95_{-0.08}^{+0.21}$  and column density  $N_{\text{H}} = (7.5 \pm 2.1) \times 10^{20}$   $\text{cm}^{-2}$ . The X-ray light curve along with the  $\Gamma_X$  evolution is shown in Fig.3. About 1000 seconds after the BAT trigger, another component emerged which is likely a normal decay and post-jet break. We used a broken power law to fit this component and found  $\alpha_3 \sim 0.45$ ,  $\alpha_4 \sim 3.5$  with break time around 35000 seconds. We follow the method discussed in Zhang et al. (2007) to calculate  $E_{\text{K,iso}}$ , which is almost constant during the normal decay phase in X-ray afterglow. We assume that it is in the  $\nu > \max(\nu_m, \nu_c)$  region, where the afterglow flux expression does not depend on the medium density. In our calculations, the microphysics parameters of the shock are assigned standard values derived from observations, i.e.  $\epsilon_e = 0.01$  and  $\epsilon_B = 0.001$ , and thus  $E_{\text{K,iso}} \sim 8 \times 10^{52}$  erg. If the later break is assumed to be a post-jet break<sup>11</sup>, one can estimate the jet opening angle  $\theta_j \sim 0.063$  rad  $\sim 3.6$  degrees with medium density  $n = 0.1 \text{ cm}^{-3}$ .

The XRT light curve of short GRB 160821B that has a short plateau emission following an abrupt decay is unusual, but not odd. This temporal behavior is similar to short GRB 090515 (Rowlinson et al. 2010). In Figure 5(a), we collect all of the short GRB light curves without extended emission to compare with the X-ray emission of GRB 160821B. We found that most short GRBs appeared to have a steeper decay around several hundred seconds. Particularly, the X-ray emission behavior of GRB 160821B is similar to GRB 090515, which is the first short GRB claimed to have a magnetar central engine origin (Rowlinson et al. 2010). Also, the plateau flux of GRB 160821B is the highest compared to other short GRBs. In Figure 5(b), we show the fluence in the BAT band (15–150 keV) and flux in the XRT band (0.3–10 keV) at  $T_0 + 100$  s for all the short GRBs in the *Swift* sample. GRB 160821B is shown with a filled circle. As expected, the higher fluence GRBs tend to have higher flux X-ray afterglows.

### 3. THE CENTRAL ENGINE OF GRB 160821B

The abrupt decay following the bright X-ray plateau observed in GRB 160821B is difficult to explain by invoking the external shock model of the black hole central engine. It must invoke the contributions from internal dissipation of a central engine. In this section, we propose the use of the millisecond magnetar central engine model to explain the abrupt decay behavior in the X-ray afterglow emission, and constrain the parameters of the magnetar.

#### 3.1. Magnetar central engine

According to Zhang & Mészáros (2001), the characteristic spin down luminosity  $L_0$  and time scale  $\tau$  are

<sup>11</sup> The error bar of the last X-ray data point is large and thus it is difficult to identify where the jet break occurs. However, it is possible to provide a lower limit to the jet opening angle if we assume that it is a jet break.

written:

$$L_0 = 1.0 \times 10^{49} \text{ erg s}^{-1} (B_{\text{p},15}^2 P_{0,-3}^{-4} R_6^6), \quad (2)$$

$$\tau = 2.05 \times 10^3 \text{ s} (I_{45} B_{\text{p},15}^{-2} P_{0,-3}^2 R_6^{-6}), \quad (3)$$

where  $I$  is the moment of inertia of a typical NS with mass  $M_{\text{NS}} = 1.4M_{\odot}$ ,  $P_0$  is the initial spin period,  $B_{\text{p}}$  is the magnetic field strength,  $R$  is the radius of the NS, and the convention  $Q = 10^x Q_x$  is adopted in cgs units for all other parameters throughout the paper. The spin-down time scale can be generally identified as the lower limit of the observed break time, i.e.

$$\tau > t_b / (1 + z), \quad (4)$$

where  $t_b$  is the break time after the internal plateau found using a broken power-law function fitting. A redshift  $z = 0.16$  is adopted. The bolometric luminosity at the break time  $t_b$  is:

$$L_b = 4\pi D_L^2 F_b \cdot k, \quad (5)$$

where  $F_b = (1.6 \pm 0.82) \times 10^{-9} \text{ erg cm}^{-2} \text{ s}^{-1}$  is the X-ray flux at  $t_b$ ,  $D_L^2$  is luminosity distance, and  $k$  is  $k$ -correction factor. The characteristic spin-down luminosity is essentially the plateau luminosity, which may be estimated as

$$L_0 \simeq L_b = (1.8 \pm 0.6) \times 10^{48} \text{ erg s}^{-1}. \quad (6)$$

Based on Equation (2) and Equation (3), one can derive the magnetar parameters  $B_{\text{p}}$  and  $P_0$ :

$$B_{\text{p},15} = 2.05 (I_{45} R_6^{-3} L_{0,49}^{-1/2} \tau_3^{-1}) \text{ G}, \quad (7)$$

$$P_{0,-3} = 1.42 (I_{45}^{1/2} L_{0,49}^{-1/2} \tau_3^{-1/2}) \text{ s}. \quad (8)$$

Using the lower limit of  $\tau$  we derive upper limits for  $P_0$  and  $B_{\text{p}}$ , which are respectively  $P_0 < 8.5 \times 10^{-3} \text{ s}$  and  $B_{\text{p}} < 3.12 \times 10^{16} \text{ G}$ . Figure 6a shows the  $B_{\text{p}} - P_0$  diagram for GRB 160821B, and compares other short GRBs.

### 3.2. Equation of state of NS

Another relevant timescale is the collapse time of a supra-massive magnetar,  $t_{\text{col}}$ . The post-internal plateau decay slope  $\alpha_2$  is steeper than 2, which is the standard spin down luminosity evolution with time (Zhang & Mészáros, 2001). The break time is therefore defined by the collapse time  $t_{\text{col}}$ , and one can write

$$\tau \simeq t_b. \quad (9)$$

The maximum gravitational mass ( $M_{\text{max}}$ ) depends on spin period which increases with time. Using the same method description in Lasky et al. (2014) and Lü et al. (2015), we can write down  $t_{\text{col}}$  as a function of  $M_{\text{p}}$

$$\begin{aligned} t_{\text{col}} &= \frac{3c^3 I}{4\pi^2 B_{\text{p}}^2 R^6} \left[ \left( \frac{M_{\text{p}} - M_{\text{TOV}}}{\hat{\alpha} M_{\text{TOV}}} \right)^{2/\hat{\beta}} - P_0^2 \right] \\ &= \frac{\tau}{P_0^2} \left[ \left( \frac{M_{\text{p}} - M_{\text{TOV}}}{\hat{\alpha} M_{\text{TOV}}} \right)^{2/\hat{\beta}} - P_0^2 \right]. \end{aligned} \quad (10)$$

where  $\hat{\alpha}$ ,  $\hat{\beta}$ , and  $M_{\text{TOV}}$  are dependent on the equation of state. Therefore we can use  $t_{\text{col}}$  to constrain

the NS equation of state (EOS). Here, we only consider five EOS (SLy, APR, GM1, AB-N, and AB-L) for the given proto-magnetar mass distribution derived from the total mass distribution of Galactic NS-NS binary systems (Fig.6b). (1) SLy: is effective nuclear interaction by neutron rich matter with  $M_{\text{TOV}} = 2.05M_{\odot}$  and  $R = 9.97\text{km}$ . (2) APR: assume that the inner material is included both dense nucleon admixture of quark matter, with  $M_{\text{TOV}} = 2.20M_{\odot}$  and  $R = 10.00\text{km}$ . (3) GM1: by relating scalar and vector couplings of the hyperons for saturated nuclear matter with  $M_{\text{TOV}} = 2.37M_{\odot}$  and  $R = 12.05\text{km}$ . (4) AB-N: neutrons nuclear attraction due to pion exchange tensor with  $M_{\text{TOV}} = 2.67M_{\odot}$  and  $R = 12.90\text{km}$ . (5) AB-L: neutrons nuclear attraction due to scalar exchange with  $M_{\text{TOV}} = 2.71M_{\odot}$  and  $R = 13.70\text{km}$  (Lasky et al. 2014). Our results show that the GM1 model gives an  $M_{\text{p}}$  band falling within the  $2\sigma$  region of the protomagnetar mass distribution, such that the GM1 EOS is the best candidate for a non-rotating NS with maximum mass  $M_{\text{TOV}} = 2.37M_{\odot}$ .

### 3.3. The energy budget of magnetar

One of the most important necessary conditions of a magnetar central engine candidate for GRBs is that the sum of the prompt emission energy ( $E_{\gamma,\text{iso}}$ ), internal plateau energy ( $E_{\text{X,iso}}$ ), and kinetic energy ( $E_{\text{K,iso}}$ ) after jet correction should be less than the total rotation energy (energy budget of magnetar) if we assume the magnetar wind is isotropic. The total rotation energy of the millisecond magnetar is

$$E_{\text{rot}} = \frac{1}{2} I \Omega_0^2 \simeq 2 \times 10^{52} \text{ erg } M_{1.4} R_6^2 P_{0,-3}^{-2}, \quad (11)$$

where  $\Omega_0 = 2\pi/P_0$  is the initial angular frequency of the neutron star. The total energy of the prompt emission is  $E_{\gamma,\text{iso}} = (2.1 \pm 0.2) \times 10^{50} \text{ erg}$  within the energy range 8-1000 keV. The X-ray internal plateau energy can be roughly estimated using the break time and break luminosity (Lü & Zhang 2014), i.e.

$$\begin{aligned} E_{\text{X,iso}} &\simeq L_b \cdot \frac{t_b}{1+z} \\ &\simeq (2.79 \pm 0.9) \times 10^{49} \text{ erg}. \end{aligned} \quad (12)$$

To estimate the kinetic energy  $E_{\text{K,iso}}$ , which is used in the standard forward afterglow model, one has  $E_{\text{K,iso}} \sim 8 \times 10^{52} \text{ erg}$  (see section 2.3). Therefore  $E_{\text{rot}} \gg \frac{1}{2} \theta_j^2 (E_{\gamma,\text{iso}} + E_{\text{X,iso}} + E_{\text{K,iso}})$ , which satisfies the magnetar central engine energy budget requirement.

## 4. GRAVITATIONAL WAVE CONSTRAINTS

### 4.1. Ellipticity constraints of newly-born NS

The coalescence of double neutron stars is believed to be one of the most likely sources for powering gravitational wave radiation with associated EM signals. These events have promising detectability prospects with current and future gravitational wave detectors like advanced LIGO/Virgo (Zhang 2013; Gao et al. 2013; Yu et al. 2013; Fan et al. 2013). If indeed a magnetar drove GRB 160821B, why was the total rotation energy of the magnetar much larger than the sum of the prompt emission energy, internal energy and kinetic energy? Several possible reasons may be used in interpret-

ing the gap in the energy compared to the energy budget. One is that the efficiency is as low as  $\sim 0.01$ , such low efficiency may disfavor the magnetic energy dissipation process (Fan et al. 2013). Another possibility is the missing energy must have been carried away by non-electromagnetic gravitational wave radiation (Fan et al. 2013; Lasky & Glampedakis 2016; Ho 2016), or carried to the black hole before spin down.

Following Fan et al. (2013) and Lasky & Glampedakis (2016), a magnetar loses rotational energy through two channels: magnetic dipole torques ( $L_m$ ) gravitational wave radiation ( $L_w$ )

$$\begin{aligned} -dE_{\text{rot}}/dt &= L_m + L_w \\ &= \frac{B_p^2 R^6 \Omega^4}{6c^3} + \frac{32GI^2 \epsilon^2 \Omega^6}{5c^5}, \end{aligned} \quad (13)$$

where  $\epsilon = 2(I_{xx} - I_{yy})/(I_{xx} + I_{yy})$  is the ellipticity in terms of the principal moments of inertia, assuming the magnetar has a triaxial shape. Following the method of Lasky & Glampedakis (2016), GW radiation can be more efficient than magnetic dipole radiation because of its stronger dependence on the neutron star spin rate  $\Omega$ , i.e.  $\Omega^6$  and  $\Omega^4$  respectively. The upper limit on the ellipticity ( $\epsilon$ ) can be expressed simply with a dependence on observed plateau luminosity and break time (Lasky & Glampedakis 2016),

$$\begin{aligned} \epsilon_{\text{obs}} &\leq \left( \frac{15c^5 \eta I}{512GL_0^2 t_b^3} \right)^{1/2} \\ &= 0.33\eta \left( \frac{I}{10^{45} \text{ g cm}^2} \right)^{1/2} \left( \frac{L_0}{10^{49} \text{ erg s}^{-1}} \right)^{-1} \left( \frac{t_b}{100 \text{ s}} \right)^{-3/2}. \end{aligned} \quad (14)$$

Using the typical NS mass and radius,  $\eta = 0.1$ ,  $L_0 \sim 5.38 \times 10^{47} \text{ erg s}^{-1}$ , and  $t_b \sim 180 \text{ s}$ , one has  $\epsilon_{\text{obs}} < 0.07$ .

#### 4.2. Detection probability of gravitational wave

If most of the rotation energy is released via gravitational wave radiation with a frequency  $f$ , the gravitational wave strain for a rotating neutron star at distance  $D_L$  can be expressed as

$$h(t) = \frac{4GI\epsilon}{D_L c^4} \Omega(t)^2. \quad (15)$$

The noise power spectral density of the detector,  $S_h(f)$ , and the stationary phase approximation implies  $\tilde{h}(f)^2 = h(t)^2 |dt/df|$ , where  $\tilde{h}(f)$  is the Fourier transform of  $h(t)$ . Following method of Lasky & Glampedakis (2016),  $\tilde{h}(f)$  can be expressed as

$$\begin{aligned} \tilde{h}(f) &= \frac{1}{D_L} \sqrt{\frac{5GI}{2c^3 f}} \\ &\approx 2.6 \times 10^{-25} \left( \frac{I}{10^{45} \text{ g cm}^2} \frac{1 \text{ kHz}}{f} \right)^{1/2} \left( \frac{D_L}{100 \text{ Mpc}} \right)^{-1}. \end{aligned} \quad (16)$$

So  $\tilde{h}(f)$  is independent of the neutron star ellipticity, but depends on the angular frequency evolution with time.

The characteristic amplitude  $h_c = fh(t)\sqrt{dt/df} = f\tilde{h}(f)$  (Corsi & Mészáros 2009; Hild et al. 2011) is

$$\begin{aligned} h_c &= \frac{f}{D_L} \sqrt{\frac{5GI}{2c^3 f}} \\ &\approx 8.22 \times 10^{-24} \left( \frac{I}{10^{45} \text{ g cm}^2} \frac{f}{1 \text{ kHz}} \right)^{1/2} \left( \frac{D_L}{100 \text{ Mpc}} \right)^{-1}. \end{aligned} \quad (17)$$

For GRB 160821B, its redshift  $z = 0.16$  corresponds to  $D_L = 765 \text{ Mpc}$ . Using this and  $f = 1000 \text{ Hz}$ , one can estimate the maximum value of the strain  $h_c$ , which is less than  $1.1 \times 10^{-24}$ . In Fig.7, we plot the gravitational wave strain sensitivity for advanced-LIGO and Einstein Telescope (ET), from Figure 3 of Lasky & Glampedakis (2016). It is clear that the strain of GRB 160821B is below the initial LIGO or advanced-LIGO noise curve. However, it is comparable to the proposed detectability limit of ET and such a signal may be detected by ET in the future.

On the other hand, keeping the total energy constant and moving the event to a lower redshift allows one to estimate the minimum detectability distance of such an event. The gravitational wave strain amplitude will be stronger if the event occurs at a lower redshift. One can estimate the cosmological distances the gravitational wave signal can be detected by current advanced-LIGO. We simulate this source at different distances and calculate the GW strain amplitude. Then we compare that value with the current sensitivity of advanced-LIGO. We find that this GW signal could be detected if shifted to about 100 Mpc, which corresponds to redshift  $z \sim 0.023$  (Fig. 7).

## 5. CONCLUSIONS AND DISCUSSION

GRB 160821B is a short gamma-ray burst (GRB) of duration less than 1 second, at redshift  $z = 0.16$ , observed by *Swift* and *Fermi*. We presented a broadband analysis of its prompt and afterglow emission and found that there is no evidence to for any ‘‘extended emission’’ up to more than 100 seconds in *Swift*/BAT and *Fermi*/GBM<sup>12</sup>. More interestingly, the X-ray plateau was followed by an extremely steep decay as observed by *Swift*/XRT but which is not unique in the *Swift* era, i.e. it is similar to GRB 090515 (Rowlinson et al. 2010), which was the first short GRB with such behavior. This behavior is very difficult to explain with the standard external shock model of black hole central engine, but could be consistent with the prediction of a magnetar central engine. It is likely that it formed into supra-massive NS initially and collapsed into black hole after several hundred seconds. This event is thus one important probe for studying the physical properties of the central engine and progenitor of GRBs.

Our analysis shows the initial short plateau emission in its X-ray lightcurve, which is consistent with energy injection from the magnetar wind of a supra-massive magnetar losing rotation energy, and followed by a steeper decay due to the magnetar collapsing to a black hole. The derived magnetar surface magnetic field  $B_p$  and the

<sup>12</sup> Presence or absence of extended emission of short GRB may be related to different physics process.

initial spin period  $P_0$  fall into a reasonable range, i.e.  $B_p < 3.12 \times 10^{16}$  and  $GP_0 < 8.5 \times 10^{-3}$  s. Using the collapse time to constrain the equation of state of the neutron star shows consistency with the GM1 model with  $M_{\text{TOV}} \sim 2.37M_\odot$ . The total isotropic-equivalent electromagnetic energy ( $\gamma$ -ray energy, internal plateau energy, and kinetic energy) is much less than the energy budget of the magnetar (a few  $\times 10^{52}$  erg), suggesting that the missing energy of the supra-massive magnetar may be radiated via gravitational waves, or carried into the black hole before spin down. If it is indeed that the energy dissipated via gravitational waves, one can constrain the ellipticity of the NS to  $\epsilon < 0.07$ . Also, the upper limit of the gravitational wave strain can be estimated as  $h_c \approx 1.1 \times 10^{-24}$  at  $f = 1000$  Hz, which is below the advanced-LIGO noise curve, but may be detectable by Einstein Telescope in the future. If we shift this source to  $\sim 100$  Mpc cosmological distance ( $z \sim 0.023$ ), then the gravitational wave signal could be detected by the current advanced-LIGO.

The event rate density of SGRBs depends on the minimum luminosity threshold. Given the detectability horizon of advanced-LIGO, i.e. a distance of 100 Mpc, all the observed SGRBs are above the BAT sensitivity. Following the method of Sun et al. (2015), if we consider the minimum isotropic luminosity of the observed SGRBs, which gives an event rate of  $4.2_{-1.0}^{+1.3}$  Gpc $^{-3}$  yr $^{-1}$  above  $7 \times 10^{49}$  erg s $^{-1}$  and varies by a factor less than two for different delay timescale models, we estimate there are 2 SGRBs every one hundred years within 100 Mpc. This is quite small and consistent with the non-detection of any SGRBs accompanying detected GW events. It is also possible that there may be low-luminosity SGRBs extending to a luminosity of  $10^{47}$  erg s $^{-1}$ , which is the detection limit for *Swift*/BAT for SGRBs at 100 Mpc. The estimated event rate density above this luminosity threshold is much larger than that of the  $7 \times 10^{49}$  erg s $^{-1}$  luminosity threshold. In this case, one may expect one low luminosity SGRB every two years. However, this is quite speculative as we have not seen any low luminosity SGRBs yet. We have already had a few such cases for

LGRBs. Both of the two cases can be tested with future detections. For current circumstances, the first scenario is preferred.

On the other hand for NS-NS mergers a more isotropic, sub-relativistic outflow could be ejected during a neutron-rich merger which can synthesize heavier radioactive elements via r-process. A thermal UV-optical transient may be powered by radioactive decay except the short GRB and its X-ray afterglow (Li & Paczynski 1998; Rezzolla et al. 2011; Yu et al. 2013). However, if the post-merger product is a supra-massive NS supported by rigid rotation, e.g. GRB 160821B, the spin-down magnetic dipole radiation of the NS remnant provides an additional energy source to the ejecta. This optical transient (Li-Paczynski-nova, macro-nova, kilonova, merger-nova, r-process) emission component would be significantly enhanced since it is heated by the magnetar wind and could easily exceed the r-process power (Li & Paczynski 1998; Tanvir et al. 2013; Berger et al. 2013; Yu et al. 2013; Yang et al. 2015; Gao, Zhang & Lü 2016; Gao et al. 2016). From the theoretical point of view, it is expected that the optical or near-infrared bump is detected at late time or an excess of flux would be visible in the spectral energy distribution. One can use the properties of observed merger-nova to constrain the parameters of the central engine. However, due to lack of optical observations, catching the possible merger-nova is expected by following up with an optical instrument in the future, i.e. Hubble Space Telescope (HST).

We acknowledge the use of the public data from the *Swift*, *Fermi* data archive, and the UK *Swift* Science Data Center. We also thank the anonymous referees for helpful comments. This work is supported by the National Basic Research Program (973 Programme) of China 2014CB845800, the National Natural Science Foundation of China (Grant No.11603006, 11533003, 11503011), the One-Hundred-Talents Program of Guangxi colleges, Guangxi Science Foundation (grant No. 2016GXNSFCB380005, 2013GXNSFFA019001), Scientific Research Foundation of GuangXi University (Grant No XGZ150299).

## REFERENCES

- Abbott, B. P., Abbott, R., Abbott, T. D., et al. 2016a, *Physical Review Letters*, 116, 061102
- Abbott, B. P., Abbott, R., Abbott, T. D., et al. 2016b, *Physical Review Letters*, 116, 241103
- Atwood, W. B., Abdo, A. A., Ackermann, M., et al. 2009, *ApJ*, 697, 1071
- Barthelmy, S. D., Chincarini, G., Burrows, D. N., et al. 2005, *Nature*, 438, 994
- Berger, E., Fong, W., & Chornock, R. 2013, *ApJ*, 774, L23
- Berger, E., Price, P. A., Cenko, S. B., et al. 2005, *Nature*, 438, 988
- Berger, E. 2014, *ARA&A*, 52, 43
- Breeveld, A. A., et al. 2016, GRB Coordinates Network, 19839, 1
- Bucciantini, N., Metzger, B. D., Thompson, T. A., & Quataert, E. 2012, *MNRAS*, 419, 1537
- Connaughton, V., Burns, E., Goldstein, A., et al. 2016, *ApJ*, 826, L6
- Corsi, A., & Mészáros, P. 2009, *ApJ*, 702, 1171
- Dai, Z. G., & Lu, T. 1998a, *Physical Review Letters*, 81, 4301
- Dai, Z. G., & Lu, T. 1998b, *A&A*, 333, L87
- Du, S., Lü, H.-J., Zhong, S.-Q., & Liang, E.-W. 2016, *MNRAS*, 462, 2990
- Duez, M. D., Liu, Y. T., Shapiro, S. L., Shibata, M., & Stephens, B. C. 2006, *Physical Review Letters*, 96, 031101
- Eichler, D., Livio, M., Piran, T., & Schramm, D. N. 1989, *Nature*, 340, 126
- Evans, P. A., et al. 2016, GRB Coordinates Network, 19837, 1
- Fan, Y.-Z., Wu, X.-F., & Wei, D.-M. 2013, *Phys. Rev. D*, 88, 067304
- Fan, Y., & Piran, T. 2006, *MNRAS*, 369, 197
- Fong, W., Berger, E., & Fox, D. B. 2010, *ApJ*, 708, 9
- Fong, W., Margutti, R., Chornock, R., et al. 2016, arXiv:1608.08626
- Fox, D. B., Frail, D. A., Price, P. A., et al. 2005, *Nature*, 437, 845
- Gao, H., Ding, X., Wu, X.-F., Zhang, B., & Dai, Z.-G. 2013, *ApJ*, 771, 86
- Gao, H., Zhang, B., & Lü, H.-J. 2016, *Phys. Rev. D*, 93, 044065
- Gao, H., Zhang, B., Lü, H.-J., & Li, Y. 2016, arXiv:1608.03375
- Gehrels, N., Norris, J. P., Barthelmy, S. D., et al. 2006, *Nature*, 444, 1044
- Gehrels, N., Sarazin, C. L., O'Brien, P. T., et al. 2005, *Nature*, 437, 851
- Giacomazzo, B., & Perna, R. 2013, *ApJ*, 771, L26
- Hild, S., Abernathy, M., Acernese, F., et al. 2011, *Classical and Quantum Gravity*, 28, 094013
- Ho, W. C. G. 2016, *MNRAS*, 463, 489

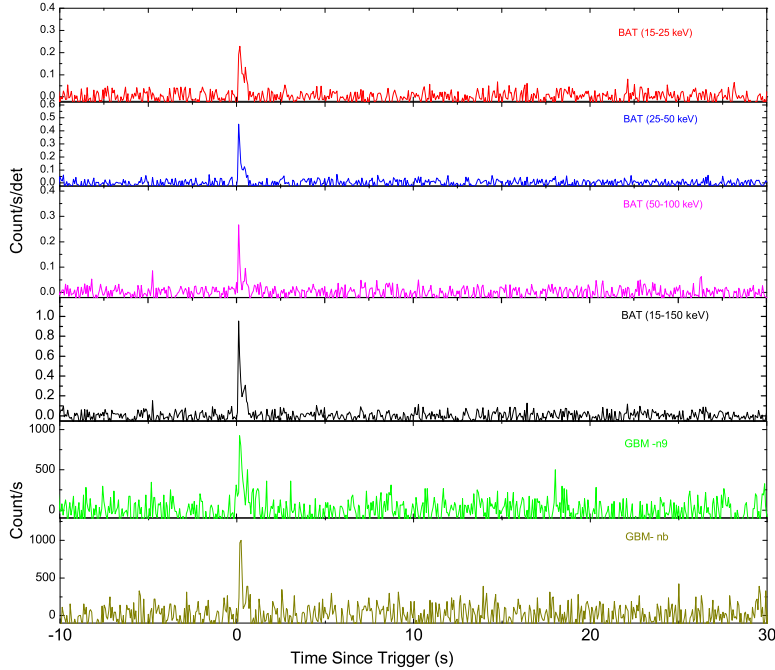


FIG. 1.— The *Swift*/BAT and *Fermi*/GBM lightcurve of GRB 160821B in different energy bands with 64 ms time bin.

- Howell, E., Regimbau, T., Corsi, A., Coward, D., & Burman, R. 2011, *MNRAS*, 410, 2123
- Kouveliotou, C., Meegan, C. A., Fishman, G. J., et al. 1993, *ApJ*, 413, L101
- Lasky, P. D., & Glampedakis, K. 2016, *MNRAS*, 458, 1660
- Lasky, P. D., Haskell, B., Ravi, V., Howell, E. J., & Coward, D. M. 2014, *Phys. Rev. D*, 89, 047302
- Lattimer, J. M., & Prakash, M. 2004, *Science*, 304, 536
- Levan, A. J., et al. 2016, *GRB Coordinates Network*, 19846, 1
- Li, L.-X., & Paczyński, B. 1998, *ApJ*, 507, L59
- Liang, E.-W., Zhang, B.-B., Stamatikos, M., et al. 2006, *ApJ*, 653, L81
- Liang, E.-W., Zhang, B.-B., & Zhang, B. 2007, *ApJ*, 670, 565
- Lorimer, D. R., Bailes, M., McLaughlin, M. A., Narkevic, D. J., & Crawford, F. 2007, *Science*, 318, 777
- Lü, H.-J., & Zhang, B. 2014, *ApJ*, 785, 74
- Lü, H.-J., Zhang, B., Lei, W.-H., Li, Y., & Lasky, P. D. 2015, *ApJ*, 805, 89
- Lyons, N., O'Brien, P. T., Zhang, B., et al. 2010, *MNRAS*, 402, 705
- Meegan, C., Lichti, G., Bhat, P. N., et al. 2009, *ApJ*, 702, 791-804
- Metzger, B. D., & Berger, E. 2012, *ApJ*, 746, 48
- Metzger, B. D., Giannios, D., Thompson, T. A., Bucciantini, N., & Quataert, E. 2011, *MNRAS*, 413, 2031
- Metzger, B. D., Quataert, E., & Thompson, T. A. 2008, *MNRAS*, 385, 1455
- Norris, J. P., & Bonnell, J. T. 2006, *ApJ*, 643, 266
- Norris, J. P., Marani, G. F., & Bonnell, J. T. 2000, *ApJ*, 534, 248
- Paczynski, P. 1986, *Nature*, 324, 392
- Paczynski, B., 1991, *AcA*, 41, 257
- Palmer, D. M., et al. 2016, *GRB Coordinates Network*, 19844, 1
- Ravi, V., & Lasky, P. D. 2014, *MNRAS*, 441, 2433
- Rezzolla, L., Giacomazzo, B., Baiotti, L., et al. 2011, *ApJ*, 732, L6
- Roming, P. W. A., Kennedy, T. E., Mason, K. O., et al. 2005, *Space Sci. Rev.*, 120, 95
- Rosswog, S., Ramirez-Ruiz, E., & Davies, M. B. 2003, *MNRAS*, 345, 1077
- Rowlinson, A., O'Brien, P. T., Metzger, B. D., Tanvir, N. R., & Levan, A. J. 2013, *MNRAS*, 430, 1061
- Rowlinson, A., O'Brien, P. T., Tanvir, N. R., et al. 2010, *MNRAS*, 409, 531
- Sakamoto, T., Hill, J. E., Yamazaki, R., et al. 2007, *ApJ*, 669, 1115
- Sari, R., Piran, T., & Narayan, R. 1998, *ApJ*, 497, L17
- Siegel, M. H., et al. 2016, *GRB Coordinates Network*, 19833, 1
- Stanbro, M., et al. 2016, *GRB Coordinates Network*, 19843, 1
- Sun, H., Zhang, B., & Li, Z. 2015, *ApJ*, 812, 33
- Tanvir, N. R., Levan, A. J., Fruchter, A. S., et al. 2013, *Nature*, 500, 547
- Thompson, C. 1994, *MNRAS*, 270, 480
- Troja, E., Cusumano, G., O'Brien, P. T., et al. 2007, *ApJ*, 665, 599
- Ukwatta, T. N., Stamatikos, M., Dhuga, K. S., et al. 2010, *ApJ*, 711, 1073
- Usov, V. V. 1992, *Nature*, 357, 472
- Xiong, S. 2016, arXiv:1605.05447
- Xu, D., et al. 2016, *GRB Coordinates Network*, 19834, 1
- Yang, B., Jin, Z.-P., Li, X., et al. 2015, *Nature Communications*, 6, 7323
- Yu, Y.-W., Zhang, B., & Gao, H. 2013, *ApJ*, 776, L40
- Zhang, B. 2016, *ApJ*, 827, L31
- Zhang, B. 2014, *ApJ*, 780, L21
- Zhang, B. 2013, *ApJ*, 763, L22
- Zhang, B. 2011, *Comptes Rendus Physique*, 12, 206
- Zhang, B., Liang, E., Page, K. L., et al. 2007, *ApJ*, 655, 989
- Zhang, B., & Mészáros, P. 2001, *ApJ*, 552, L35
- Zhang, B., Zhang, B.-B., Virgili, F. J., et al. 2009, *ApJ*, 703, 1696
- Zhang, S.-N., Liu, Y., Yi, S., Dai, Z., & Huang, C. 2016, arXiv:1604.02537

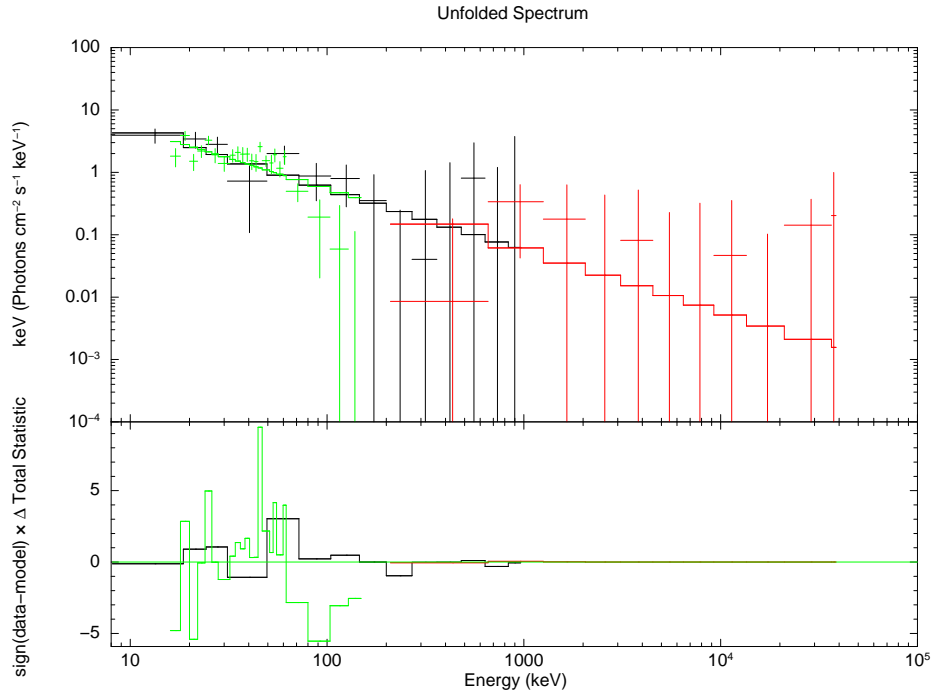


FIG. 2.— Joint fit of the time-averaged spectra of BAT (green points) and GBM (red and black points) data with a power-law model.

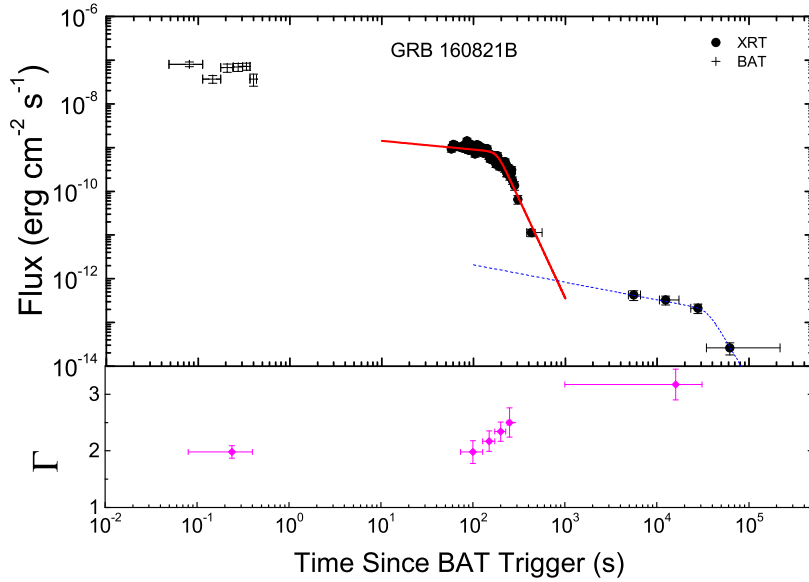


FIG. 3.— The *Swift*/XRT light curve of GRB 160821B (black points). The **lower** plot shows the photon index evolution. The red solid line and blue dashed line show the broken power-law fit to the light curve.



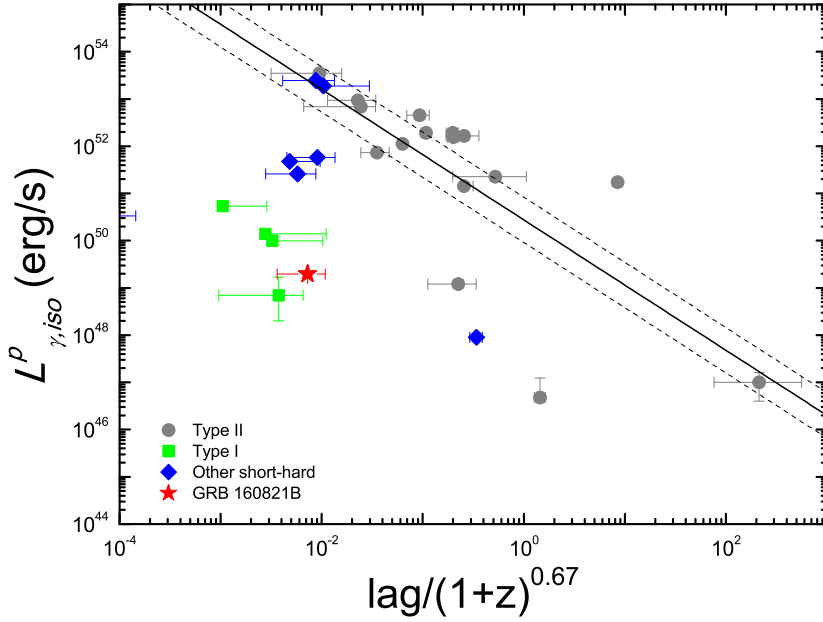


FIG. 4.— Luminosity-spectral lag diagram. The red star indicates GRB 160821B. Grey dots, green squares, and blue diamonds are indicated Type II, Type I, and other-short hard GRBs, respectively. The solid black line and two dash lines are represented the best linear fit to type II GRBs and  $2\sigma$  region.

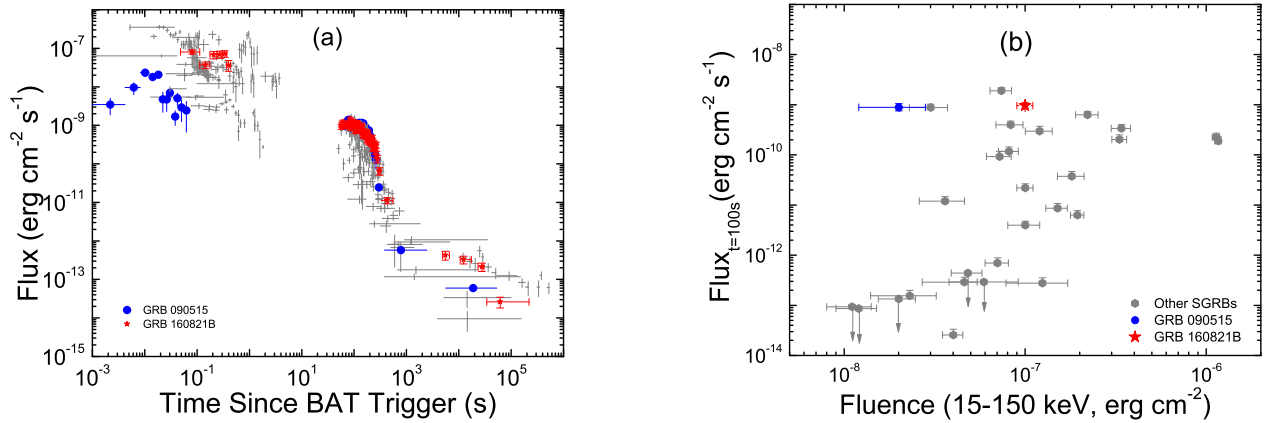


FIG. 5.— (a): Comparing the X-ray light curve (0.3–10 keV) of GRB 160821B with other short GRBs without extended emission. (b): The fluence in BAT energy band (15–150 keV) versus the flux in XRT band (0.3–10 keV) for all Swift SGRBs which were observed 100s after the trigger time. The red star marks the location of GRB 160821B.

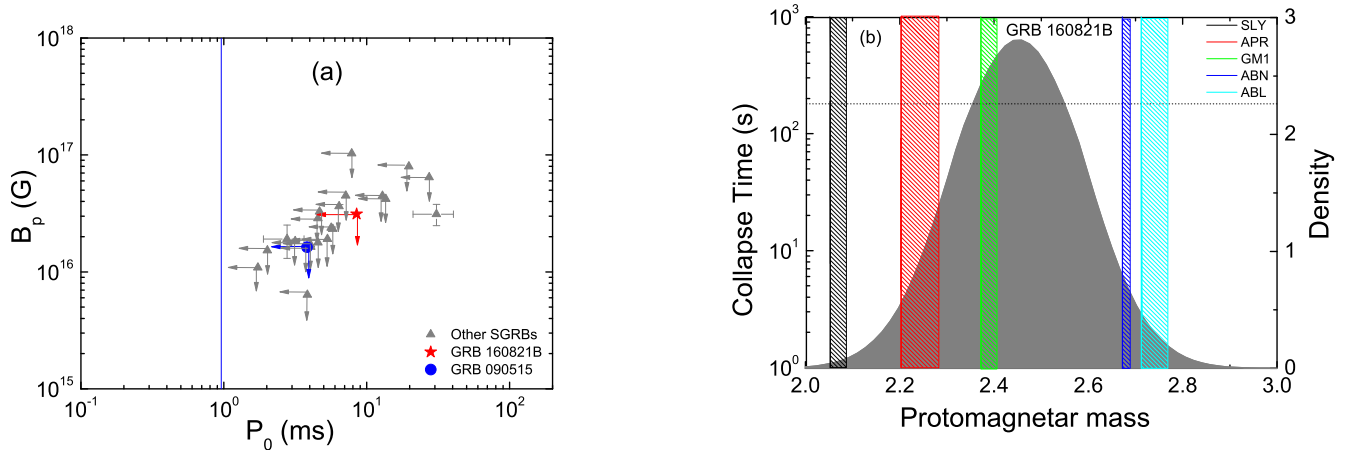


FIG. 6.— (a): Inferred magnetar parameters, initial spin period  $P_0$  vs. surface polar cap magnetic field strength  $B_p$  derived for GRB 160821B (red star), compared with other short GRBs (grey triangle) and GRB 090515 (blue point). The vertical solid line is the break-up spin period limit for a neutron star (Lattimer & Prakash 2004). (b): Collapse time as a function of the protomagnetar mass of GRB 160821B for different EOS: SLy (black), APR (red), GM1 (green), AB-N (blue), and AB-L (cyan). The horizontal dotted line is the observed collapse time.

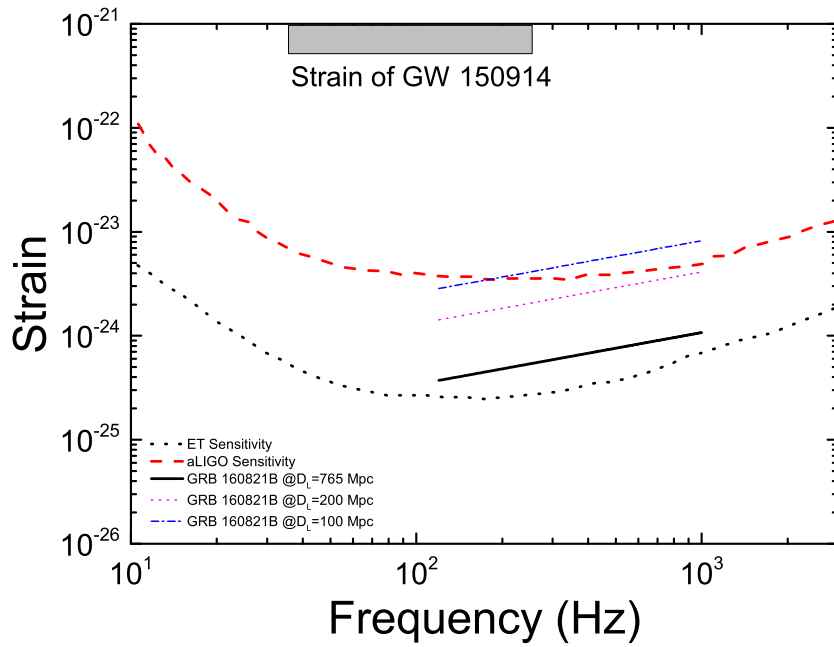


FIG. 7.— Gravitational wave strain evolution with frequency for GRB 160821B, at distance  $D_L = 765$  Mpc (black solid line), 200 Mpc (pink dot line), 100 Mpc (blue dash - dot line). The grey region is the strain of GW 150914 between 35 Hz and 250 Hz. The black dotted line and red dashed line are the sensitivity limits for aLIGO and the Einstein Telescope, respectively.